Soft Matter

PAPER

View Article Online
View Journal | View Issue

Cite this: *Soft Matter*, 2017, 13, 4607

Liquid crystalline bilayers self-assembled from rod–coil diblock copolymers

Yongqiang Cai, [a] Pingwen Zhang*[b] and An-Chang Shi *[c]

Received 20th February 2017,
Accepted 23rd May 2017

DOI: 10.1039/c7sm00354d

rsc.li/soft-matter-journal

The structure and phase behaviour of bilayer membranes self-assembled from rod–coil diblock copolymers are studied using the self-consistent field theory, focusing on the occurrence and relative stability of liquid crystalline phases induced by the geometric shape and orientational interaction of the rod-blocks. A variety of liquid crystalline bilayers, corresponding to the smectic phases in bulk systems, are predicted to occur as equilibrium phases of the system. The ordered morphologies and phase behaviour of the system are analyzed. Phase diagrams of the self-assembled bilayers are constructed. The theoretical results provide an understanding of the formation mechanisms of these intricate phases.

1 Introduction

Block copolymers are macromolecules composed of chemically distinct subchains, or blocks, tethered together by covalent bonds. The unique architecture of block copolymers leads to the formation of ordered phases composed of nanoscopic domains arranged on various lattices. The phase behaviour and ordered morphologies of block copolymers have been attracting tremendous attention since the 1970s.[1–3] Furthermore, the self-assembly of block copolymers under various confinements such as thin films and nanochannels could lead to ordered morphologies that are not obtainable in bulk systems.[4–6] Most of the previous studies were carried out on block copolymers composed of flexible or coil blocks, in which the polymeric domains are fluid-like or disordered. On the other hand, many polymers, especially conducting polymers and certain biopolymers,[7] are semiflexible or even rod-like in nature. It is well known that semiflexible and rod-like polymers tend to form liquid crystalline phases due to the geometric shape and orientational interaction intrinsic to these macromolecules. Therefore it is natural to expect that the liquid crystalline ordering of the rod blocks could have significant effects on the phase behaviors of rod–coil diblock copolymers in various states such as melts, solutions or under confinement.[7–11] In particular, previous experimental and theoretical studies have revealed that the self-assembly of rod–coil diblock copolymer melts could lead to very rich phase behaviours, exhibiting ordered phases combining the features of block copolymer microphases and liquid crystals.[7,12] The observed morphologies include, to name a few, nematic, smectic, lamellar, cylindrical, gyroid, body-centred cubic, and zigzag structures.[7,12,13] From a practical point of view, the self-assembled structures of rod–coil diblock copolymers containing conjugate blocks provide nanostructured materials for potential technological applications such as photovoltaics.[14,15]

Compared with block copolymer melts, block copolymer solutions exhibit even rich phase behaviours because of the additional degree of freedom, *viz.* polymer concentrations and polymer–solvent interactions. For dilution solutions, it has been well established that amphiphilic molecules such as lipids, surfactants and diblock copolymers in hydrophilic solvents could self-assemble to form a variety of structured aggregates, including spherical micelles, cylindrical micelles and bilayers.[16] One particularly interesting type of aggregates is the self-assembled bilayer, which could be used as mimetics for biological membranes.[17,18] In bilayer membranes the hydrophilic blocks are located on the outer surface while the hydrophobic blocks are hidden in the interior. At the molecular scale, it is expected that flexible blocks would exhibit disordered lateral arrangement in a bilayer, resulting in a fluidic or disordered bilayer membrane. On the other hand, for block copolymers with semiflexible or rigid rod blocks, the arrangement of the macromolecules inside the bilayers could exhibit orientational order due to the geometric shape and orientational interaction of the hydrophobic blocks, resulting in liquid crystalline bilayer membranes.[19] The orientational order of the rod-like blocks within a bilayer could be perpendicular or inclined to the bilayer, forming ordered membranes with structures analogous to the smectic-A or smectic-C phases, respectively. Furthermore, the spatial arrangement of the rod blocks in the smectic morphologies could assume end-to-end or interdigitated configurations. A combination of the orientational

[a] *School of Mathematical Sciences, Peking University, Beijing 100871, P. R. China. E-mail: caiyq.math@pku.edu.cn*
[b] *LMAM, CAPT and School of Mathematical Sciences, Peking University, Beijing 100871, P. R. China. E-mail: pzhang@pku.edu.cn*
[c] *Department of Physics and Astronomy, McMaster University, Hamilton, Ontario, L8S 4M1, Canada. E-mail: shi@mcmaster.ca*

and spatial arrangements of the rods within a bilayer could lead to the formation of at least four types of liquid crystalline phases, similar to the smectic phases in bulk systems.[20–22]

Theoretically, the understanding of the structure and thermodynamic behaviour of self-assembled bilayers could be obtained from generic coarse grained models of amphiphilic molecules. One commonly used model for the study of self-assembled bilayers is composed of AB diblock copolymers dissolved in A homopolymers.[23–25] The phase behaviour of rod–coil diblock copolymers in the melt state has been studied by a large number of researchers using different theoretical approaches including the asymptotic method,[20,26] Landau theory,[27] computer simulations,[28,29] mean-field theory of lattice models[30,31] and the self-consistent field theory.[22,32–37] These previous theoretical studies have revealed very rich liquid crystalline behaviours of rod–coil diblock copolymer melts. Furthermore, it has been shown that the addition of coil or rod homopolymers to a self-assembling rod–coil diblock copolymer is an effective method to induce liquid crystal phase transition and control the domain spacing of the ordered structure.[38–40] However, despite extensive experimental and theoretical studies of rod–coil diblock copolymer melts and solutions, the morphology and phase behaviour of self-assembled bilayers from rod–coil diblock copolymers remain largely unexplored.

In this paper, we report on a systematic study of the structure and phase behaviour of bilayer membranes self-assembled from rod–coil diblock copolymers using the self-consistent field theory (SCFT). It has been demonstrated that the SCFT provides a flexible and accurate framework for the study of inhomogeneous polymeric systems[41] including different micelle structures.[42] In the current study, we obtain accurate numerical solutions of the SCFT equations corresponding to various liquid crystalline bilayers, including three types of A-phase, two types of C-phase, OB-phase and P-phase, where the A-phases and C-phases are bilayer analogues of the smectic crystalline phases in bulk systems.[22,33,39] The structure and energetics of the different phases are analyzed. In particular, the effects of the conformational asymmetry between rods and coils on the structure of A-phases and C-phases are systemically studied. Phase diagrams of the bilayers are constructed by comparing the free energy of the different phases. The results reveal that various bilayer phases with different liquid crystalline order could be obtained, providing a rich library of ordered structures for potential applications of polymeric systems involving rod–coil diblock copolymers.

The rest of the paper is organized as follows. A detailed description of the SCFT model and the candidate bilayer phases are presented in Section 2. Our main results on the phase diagrams and phase transitions are given in Section 3. The final section presents some discussions relating to our results and the main conclusion from the study.

2 Model and theoretical framework

2.1 Basic model and numerical methods

The model system used in our study is a binary mixture of A (coil)–B (rod) diblock copolymers and A (coil) homopolymers. The phase behaviour of the model system is examined using the polymeric self-consistent field theory (SCFT) formulated in the grand canonical ensemble.[24,43,44] The model system is controlled by a large number of parameters. In the current study, the copolymers and the homopolymers are assumed, for simplicity, to have the same degree of polymerization N. Furthermore, we consider AB diblock copolymers with equal A and B volume fractions, $f_A = f_B = 0.5$. The interaction between A and B monomers is described by a Flory–Huggins parameter[45] χ, whereas the orientation interaction between the rods is assumed to have the Maier–Saupe form[46] with an interaction parameter η. Furthermore, the conformational asymmetry between the coil (A) and rod (B) blocks is quantified by a geometrical asymmetry parameter,[22,47] $\beta = bN/R_g$, where $R_g = \sqrt{Na^2/6}$ is the gyration radius of A-chains, and a and b are the statistical segment lengths of A (coil) and B (rod) blocks, respectively. Finally the chemical potential of the copolymers μ_c, or the corresponding activity $z_c = \exp(\mu_c)$, is used as a control parameter to regulate the average concentration of the diblock copolymers in the blends.

Within the SCFT framework, the free energy of the binary mixture is given by[41]

$$\frac{N\mathscr{F}}{k_BT\rho_0} = \int d\mathbf{r}\left[\chi N\phi_A(\mathbf{r})\phi_B(\mathbf{r}) - \sum_{\alpha=A,B}\omega_\alpha(\mathbf{r})\phi_\alpha(\mathbf{r}) + \frac{1}{2\eta N}\mathbf{M}(\mathbf{r}):\mathbf{M}(\mathbf{r}) - \xi(\mathbf{r})(\phi_A(\mathbf{r}) + \phi_B(\mathbf{r}) - 1)\right] - z_cQ_c - Q_h, \quad (1)$$

where $\phi_\alpha(\mathbf{r})$ and $\omega_\alpha(\mathbf{r})$ are the local concentration and the mean field of α-type monomers (α = A, B). The tensor field $\mathbf{M}(\mathbf{r})$ is the mean orientational field of the rod (B) blocks. The local pressure field $\xi(\mathbf{r})$ is a Lagrange multiplier introduced to enforce the incompressibility condition of the system. The last two terms in eqn (1) are contributions from the single-chain partition functions of the two polymers, Q_c and Q_h.

The fundamental quantity to be computed in the SCFT study is the polymer segment probability distribution functions (or the propagators), $q_A^h(\mathbf{r},s)$ for A homopolymers, and $q_A^\pm(\mathbf{r},s)$, $q_B^\pm(\mathbf{r},\mathbf{u},s)$ for AB diblock copolymers, where $\mathbf{u}$ is a unit orientational vector. These propagators satisfy the modified diffusion equations[41] in the presence of the mean fields (ω_A, ω_B and $\mathbf{M}$),

$$\frac{\partial}{\partial s}q_A^h(\mathbf{r},s) = (R_g^2\nabla_\mathbf{r}^2 - \omega_A(\mathbf{r}))q_A^h(\mathbf{r},s), s\in(0,1), \quad (2)$$

$$\frac{\partial}{\partial s}q_A^\pm(\mathbf{r},s) = \left(R_g^2\nabla_\mathbf{r}^2 - \omega_A(\mathbf{r})\right)q_A^\pm(\mathbf{r},s), s\in(0,f_A), \quad (3)$$

$$\frac{\partial}{\partial s}q_B^\pm(\mathbf{r},\mathbf{u},s) = \left(\pm\beta R_g\mathbf{u}\cdot\nabla_\mathbf{r} - \Gamma(\mathbf{r},\mathbf{u})\right)q_B^\pm(\mathbf{r},\mathbf{u},s), s\in(0,f_B), \quad (4)$$

with the initial conditions,

$$q_A^h(\mathbf{r},0) = 1, q_A^-(\mathbf{r},0) = 1, q_B^-(\mathbf{r},\mathbf{u},0) = \frac{1}{4\pi}, \quad (5)$$

$$q_{\mathrm{A}}^{+}(\mathbf{r},0)=\int \mathrm{d}\mathbf{u} q_{\mathrm{B}}^{-}(\mathbf{r},\mathbf{u},f_{\mathrm{B}}), q_{\mathrm{B}}^{+}(\mathbf{r},\mathbf{u},0)=\frac{1}{4\pi}q_{\mathrm{A}}^{-}(\mathbf{r},f_{\mathrm{A}}). \quad (6)$$

Here the **r**, **u**-dependent field $\Gamma(\mathbf{r},\mathbf{u})$ is defined by

$$\Gamma(\mathbf{r},\mathbf{u})=\omega_{\mathrm{B}}(\mathbf{r})-\mathbf{M}(\mathbf{r}):\left(\mathbf{uu}-\frac{1}{3}\mathbf{I}\right). \quad (7)$$

In terms of the chain propagators, the single-chain partition functions are given by

$$Q_{\mathrm{c}}=\int \mathrm{d}\mathbf{r} q_{\mathrm{A}}^{+}(\mathbf{r},f_{\mathrm{A}}), \quad (8)$$

$$Q_{\mathrm{h}}=\int d\mathbf{r} q_{\mathrm{A}}^{\mathrm{h}}(\mathbf{r},1). \quad (9)$$

Furthermore, the density distributions of A and B monomers are obtained from the propagators as

$$\begin{aligned}\phi_{\mathrm{A}}(\mathbf{r}) &= \phi_{\mathrm{A}}^{\mathrm{h}}+\phi_{\mathrm{A}}^{\mathrm{c}}\\ &= \int_0^1 \mathrm{d}s q_{\mathrm{A}}^{\mathrm{h}}(\mathbf{r},s) q_{\mathrm{A}}^{\mathrm{h}}(\mathbf{r},1-s)+z_{\mathrm{c}}\int_0^{f_{\mathrm{A}}}\mathrm{d}s q_{\mathrm{A}}^{-}(\mathbf{r},s) q_{\mathrm{A}}^{+}(\mathbf{r},f_{\mathrm{A}}-s),\end{aligned} \quad (10)$$

$$\phi_{\mathrm{B}}(\mathbf{r})=4\pi z_{\mathrm{c}}\int_0^{f_{\mathrm{B}}}\mathrm{d}s\int \mathrm{d}\mathbf{u} q_{\mathrm{B}}^{-}(\mathbf{r},\mathbf{u},s) q_{\mathrm{B}}^{+}(\mathbf{r},\mathbf{u},f_{\mathrm{B}}-s). \quad (11)$$

Finally the orientational order parameter of B blocks is given by

$$\mathbf{S}(\mathbf{r})=4\pi z_{\mathrm{c}}\int_0^{f_{\mathrm{B}}}\mathrm{d}s\int \mathrm{d}\mathbf{u} q_{\mathrm{B}}^{-}(\mathbf{r},\mathbf{u},s)\left(\mathbf{uu}-\frac{\mathbf{I}}{3}\right) q_{\mathrm{B}}^{+}(\mathbf{r},\mathbf{u},f_{\mathrm{B}}-s). \quad (12)$$

The rest of the SCFT equations concerning the mean fields to the density distributions are

$$\omega_{\mathrm{A}}(\mathbf{r})=\chi N\phi_{\mathrm{B}}(\mathbf{r})-\xi(\mathbf{r}), \quad (13)$$

$$\omega_{\mathrm{B}}(\mathbf{r})=\chi N\phi_{\mathrm{A}}(\mathbf{r})-\xi(\mathbf{r}), \quad (14)$$

$$\mathbf{M}(\mathbf{r})=\eta N\mathbf{S}(\mathbf{r}), \quad (15)$$

$$\phi_{\mathrm{A}}(\mathbf{r})+\phi_{\mathrm{B}}(\mathbf{r})=1. \quad (16)$$

For a given set of control parameters, the above SCFT equations are solved to obtain solutions corresponding to different candidate phases. The free energy of the different phases is then compared to construct the phase diagram. Numerically, the SCFT equations are solved by iteration methods, whose convergence could be accelerated by the Anderson mixing.[48] The most time-consuming step of solving the SCFT equations is the computation of the propagators by solving the modified diffusion equations (MDE). When the rod-blocks are assumed to be semi-flexible, various efforts[49,50] have been devoted to develop numerical algorithms for the MDE of the wormlike chain model. In particular, the fast Fourier transform (FFT) can be used to treat the periodic boundary condition. In the current study, the compact finite difference scheme[51] is used to enforce the reflecting boundary conditions. Specifically, the partial derivative operators about **r** are treated using a fourth-order compact finite difference scheme, and the s dependence is treated using a third-order implicit Runge–Kutta method.[52] The scheme is especially suitable for the current problem, where a well-designed nonuniform grid is used to capture the sharp interface especially for large values of χN and ηN. In the current study, computation domain is constrained in one dimension and the domain size D is determined by the condition that the concentration profile near the boundaries of the computational box is the same as the bulk concentration within a prescribed error. The number of **u** grid points is 32×36, **r** grid points are changed over 200–400 and s grid points are changed over 300–800 under different model parameters to ensure that the free energy is converged in the order of 10^{-4} and the fields are self-consistent with L^2-norm error less than 10^{-6}.

2.2 Candidate phases

Because the SCFT equations are a set of non-linear and non-local equations, the SCFT equations have more than one solution. Each solution of the SCFT acts as a candidate phase. On the other hand, finding the different solutions of SCFT depends crucially on the initial configurations used in the SCFT calculations.[53,54] A popular choice is random configurations. On the other hand, it has been demonstrated by a number of researchers[53,54] that random configurations alone would lead to a limited number of candidate phases. A large number of metastable phases would be missed if one only uses a restricted set of initial configurations. In our study of the phases and phase transitions of block copolymer systems, we have used various initial configurations, including random and designed initial configurations, to obtain the candidate structures. The structure and orientational order of these candidate phases are described in this subsection.

As the simplest case, the solution of the spatially homogeneous phase of the system can be obtained analytically. Assuming that the orientational field is uniaxial, *i.e.* $\mathbf{M}(\mathbf{r})\equiv \mathrm{diag}(M, M, -2M)$, the free energy of a spatially homogeneous phase is given by

$$\frac{N\mathscr{F}_{\mathrm{bulk}}}{k_{\mathrm{B}}T\rho_0 V}=\frac{3M^2}{\eta N}+\chi N f_{\mathrm{B}}{}^2\phi_{\mathrm{bulk}}{}^2+\ln(1-\phi_{\mathrm{bulk}})-1, \quad (17)$$

where M and the bulk copolymer concentration ϕ_{bulk} are determined by a set of nonlinear equations,

$$\begin{cases}\mu_{\mathrm{c}} = \ln\phi_{\mathrm{bulk}}-\ln(1-\phi_{\mathrm{bulk}})+\chi N f_{\mathrm{B}}(1-2f_{\mathrm{B}}\phi_{\mathrm{bulk}})\\ \qquad -\ln\left(\int_0^1 \exp\left(\left(1-3x^2\right)Mf_{\mathrm{B}}\right)\mathrm{d}x\right),\\ M=\dfrac{\eta N f_{\mathrm{B}}\phi_{\mathrm{bulk}}}{6}\dfrac{\int_0^1\left(1-3x^2\right)\exp\left(\left(1-3x^2\right)Mf_{\mathrm{B}}\right)\mathrm{d}x}{\int_0^1\exp\left(\left(1-3x^2\right)Mf_{\mathrm{B}}\right)\mathrm{d}x}.\end{cases} \quad (18)$$

The second equation in eqn (18) depends only on Mf_{B} if the combination $\eta N f_{\mathrm{B}}{}^2\phi_{\mathrm{bulk}}$ is taken as a control parameter. Further analysis of the right hand side of this equation reveals that a solution with non-zero $M\neq 0$, corresponding to the nematic phase, exists only if $\eta N f_{\mathrm{B}}{}^2>6.72$. On the other hand, solutions with $M=0$, correspond to the isotropic or disordered phase, always exist. Specifically, the SCFT equations may have up to three isotropic solutions, where the solution with small ϕ_{bulk} is the hA-rich phase, and the solution with large ϕ_{bulk} is the AB-rich phase. For the given set of parameters used in our

study, the hA-rich phase has lower free energy than the AB-rich phase when $\chi N > 4 \ln z_c$.

For the inhomogeneous phases, the structure is described by the density profiles $\phi_A(\mathbf{r})$, $\phi_B(\mathbf{r})$ and the orientational order parameter $\mathbf{S}(\mathbf{r})$. In particular, the eigenvalues and eigenvectors of the orientational order parameter, $\mathbf{S}$, can be used to classify the liquid crystalline order of the self-assembled bilayers. By denoting the eigenvalues and relevant eigenvectors of $\mathbf{S}$ by λ_1, λ_2, λ_3, $\mathbf{n}_1$, $\mathbf{n}_2$, $\mathbf{n}_3$ (with $|\lambda_1| \geq |\lambda_2| \geq |\lambda_3|$), and the angle between $\mathbf{n}_1$ and the normal vector ($\mathbf{z}$) of interface by θ, a classification of the bilayer phases could be carried out according to these parameters as summarized in Table 1. In the current study, solutions of the SCFT equations, corresponding to the A, C, P (perpendicular, biaxial) and OB (oblate, uniaxial) phases, are obtained. These phases are bilayer analogues of the bulk smectic phases of rod–coil diblock copolymer melts obtained from SCFT calculations.[22,55]

The morphologies of the different liquid crystalline bilayers are obtained from the order parameter distributions. In the A-phase, corresponding to the smectic-A phase in the bulk, the rods are aligned parallel to the normal direction of the bilayer. In the C-phase, corresponding to the smectic-C phase in the bulk, the direction of the rods, $\mathbf{n}_1$, is tilted by an angle θ away from the normal direction of the bilayer. In the P-phase the local distribution of the director $\mathbf{n}_1$ is biaxial with two peaks away from the bilayer normal $\mathbf{z}$ and an average orientation $\mathbf{n}_1$ perpendicular to $\mathbf{z}$. In the OB-phase, the average orientation $\mathbf{n}_1$ is parallel to $\mathbf{z}$, but the maximal absolute eigenvalue λ_1 is negative resulting in an oblate distribution, *i.e.* the local distribution of $\mathbf{n}_1$ is very close to perpendicular to the bilayer interface. The number of possible ordered phases of a bilayer is further increased by the fact that there are different types of A and C phases depending on the alignment of the rods and the tilt angle θ of the C-phase, which might be multi-valued. The basic structure of the different ordered phases is sketched in Fig. 1. It is noted that the spatial distributions of the individual rod segments $\phi_s(\mathbf{r})$ could be computed from the propagators,[39]

$$\phi_{s_0}(\mathbf{r}) = 4\pi z_c \int d\mathbf{u} q_B^-(\mathbf{r}, \mathbf{u}, s_0) q_B^+(\mathbf{r}, \mathbf{u}, 1 - s_0). \quad (19)$$

The value of s_0 is set as f_A, $f_A + f_B/2$ and 1 separately in this paper to define ϕ_{join}, ϕ_{mid} and ϕ_{end}, representing the concentrations of the joint, middle and end segments of rod blocks.

The free energy of the different phases is obtained by inserting the SCFT solutions into the free energy functional of the system (eqn (1)). The relative stability of an ordered bilayer phase is determined by its excess free energy, *i.e.* the free energy difference between the ordered phase and the isotropic phase, $\mathscr{F} - \mathscr{F}_{bulk}$. For a planar bilayer geometry, the excess free energy ($\mathscr{F} - \mathscr{F}_{bulk}$) is proportional to the area (A) of the membrane; therefore we can define the excess free energy density as[24]

$$F_{ex} = \frac{N(\mathscr{F} - \mathscr{F}_{bulk})}{k_B T \rho_0 A}. \quad (20)$$

Similarly, the thickness of a bilayer can be defined as the copolymer excess per unit area,[24]

$$\Omega = \frac{1}{A} \int d\mathbf{r} (\phi^c(\mathbf{r}) - \phi_{bulk}), \quad (21)$$

where $\phi^c(\mathbf{r}) = \phi_A^c(\mathbf{r}) + \phi_B(\mathbf{r})$ is the local concentration of the copolymers. In what follows these quantities are used to examine the relative stability of the different phases.

Table 1 Classification of liquid crystalline bilayer structures

		$\theta = 0°$	$0° < \theta < 90°$	$\theta = 90°$
Uniaxial $\lambda_2 = \lambda_3$	$\lambda_1 > 0$	A	C	—
	$\lambda_1 < 0$	OB	—	—
Biaxial $\lambda_2 \neq \lambda_3$	$\lambda_1 > 0$	—	—	P
	$\lambda_1 < 0$	—	—	—

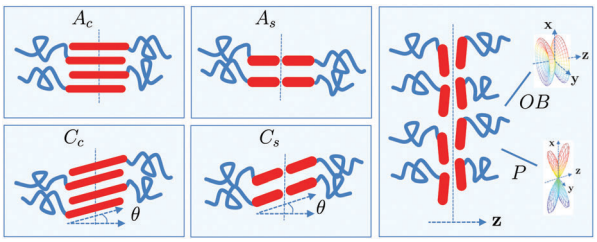

Fig. 1 Schematics of the phases of a bilayer. In the A_s and C_s phases the rods assume an end-to-end arrangement, whereas the rods assume an interdigitated arrangement in the A_c and C_c phases. When the tilt angle is multi-valued, C_c could be further differentiated as the C_A ($\theta < 45°$) and C_P ($\theta > 45°$) phases. In the OB and P phases the rods are nearly perpendicular to the bilayer normal $\mathbf{z}$, where the local distribution of the director $\mathbf{n_1}$ is oblate in the OB phase and biaxial in the P phase, as shown in the accompanying plots.

3 Liquid crystalline phases and phase diagrams of bilayers

3.1 Property of the A-phases and C-phases

In this subsection the property of a self-assembled bilayer is analyzed by examining its excess free energy, thickness and segment distributions obtained from the SCFT calculations. For rod–coil diblock copolymer melts, it has been shown that, besides the copolymer composition f, the conformational asymmetry between the rods and coils, quantified by the parameter β, greatly affects their phase behaviour.[47] It is therefore expected that the parameter β will have a strong influence on the phase behaviour of self-assembled bilayers from rod–coil diblock copolymers. In what follows, the effects of β on the property and phase behaviour of the bilayers are investigated.

3.1.1 The A-phases. As shown in Fig. 1, the A-phase of the bilayer is a liquid crystalline structure in which the rod blocks are oriented perpendicular to the bilayer. According to the spatial arrangements of the rods within a bilayer, the A-phase can be divided into a number of sub-phases, such as the A_c and A_s types illustrated in Fig. 1. In the A_c phase the rods assume a completely interdigitated arrangement, whereas the rods assume an end-to-end arrangement in the A_s phase.

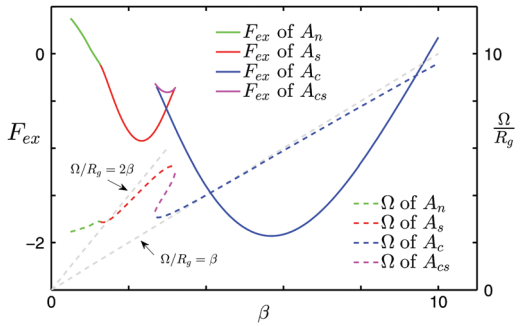

Fig. 2 Plots of the free energy density F_{ex} and bilayer thickness Ω of A-phases as a function of β with fixed χN = 15, ηN = 30, z_c = 10. Two straight lines specified by $\Omega/\beta R_g$ = 1 and 2 are shown as references.

The effect of the asymmetry parameter β on the spatial arrangements of the rods could be elucidated by the behaviour of the excess free energy and the thickness of the bilayer as a function of β. As an example, the excess free energy density (F_{ex}) and the bilayer thickness (Ω) of the A-phases are shown as a function of β in Fig. 2 with a set of parameters χN = 15, ηN = 30, z_c = 10. The first feature to notice from Fig. 2 is that the free energy and bilayer thickness as a function of β are multi-valued in certain regions of β. The stable phase is the one with the lowest free energy, and thus the triangle loop at $\beta \sim 3$ corresponds to metastable or unstable state. In particular, the structure with partially interdigitated arrangement of rods, denoted as A_{cs}, represents an unstable phase. As the value of β is increased across this transition point, the bilayer changes from the A_s phase to the A_c phase with an abrupt decrease of the bilayer thickness.

For bilayers with perfect interdigitated and end-to-end arrangements, the bilayer thickness should follow two straight lines given by $\Omega/\beta R_g$ = 1 and $\Omega/\beta R_g$ = 2. The calculated bilayer thickness curves for the A_s and A_c phases shown in Fig. 2 deviate from these two straight lines, indicating that a small degree of interdigitation of the rod blocks is present in the structures. For the case of very short rod blocks corresponding to small β, their centre of mass could have a broad distribution, resulting in a structure, termed as the A_n phase, analogous to the nematic phase in bulk liquid crystals.

The structure of the self-assembled bilayers is revealed by the spatial distribution of the rod segments. Typical segment distributions are shown in Fig. 3 for β = 3.5, 3, 2.5 and 0.5, corresponding to the different A-phases presented above. Specifically, the distributions of the joint, middle and end segments of the rod blocks are shown in Fig. 3. The interdigitate state of the different A-phases can be clearly seen from the distribution of the middle-segment of the rods, ϕ_{mid}. For the A_c phase, ϕ_{mid} is sharply peaked at the middle of the bilayer as shown in Fig. 3(a), indicating an almost completely interdigitated arrangement of the rods. For the A_s phase, ϕ_{mid} exhibits two peaks near the peaks of the joint-segment distribution as shown in Fig. 3(c), indicating an end-to-end arrangement of the rods. For the intermediate A_{cs} phase, ϕ_{mid} shows three peaks as shown in Fig. 3(b), indicating a partially interdigitated arrangement.

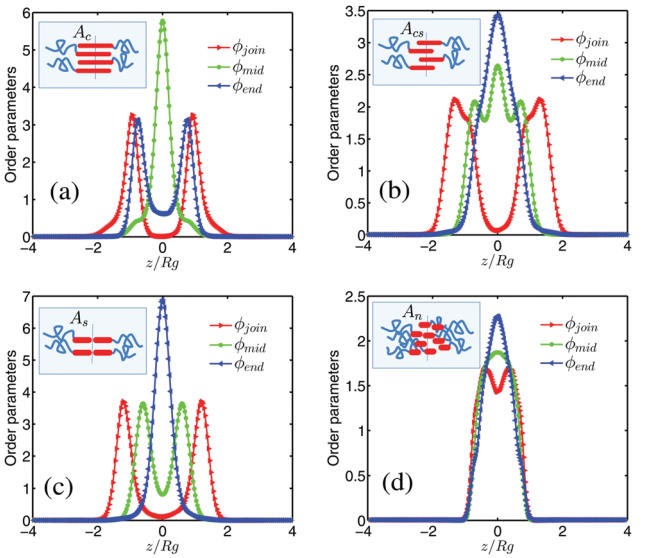

Fig. 3 The spatial distribution of the individual rod segments (join, mid and end) and the corresponding schematic of A-phases. (a) A_c phase with β = 3.5. (b) A_{cs} phase with β = 3. (c) A_s phase with β = 2.5. (d) A_n phase with β = 0.5.

These structural features are corroborated by the corresponding end-segment distribution functions (ϕ_{end}). For the A_n phase, the distribution of the middle- and end-segments exhibits one peak at the middle of the bilayer as shown in Fig. 3(d), indicating a random spatial distribution of centre of mass of the rod blocks.

The phase transformation sequence and transition boundaries are determined by the minimum of the free energy of the different phases. From the free energy curves shown in Fig. 2, a phase transition sequence from A_n to A_s to A_c for increasing β is predicted. For very small values of β, the rods are so short that their centre of mass could assume a random spatial distribution, resulting in the formation of the A_n phase. For very large values of β, the rods are long favouring a completely interdigitated spatial arrangement, leading to the formation of the A_c phase. For intermediate values of β, the spatial distribution of the rods could assume an end-to-end arrangement forming the A_s phase. It is interesting to note that, at an intermediate value of $\beta \sim 3$, A_s and A_c coexist, and the partially interdigitated structure (A_{cs}) is a metastable or unstable phase in this case.

3.1.2 The C-phases. Similar to the bulk smectic-C phase, the orientation of the rods in the C-phase of a bilayer self-assembled from rod–coil diblock copolymers is tilted away from the normal direction of the bilayer with a tilt angle θ. In this case the interdigitation and orientation of the rods are coupled, resulting in a more complex behaviour than that of the A-phases. From the perspective of the spatial arrangement of the rods, the C-phase could be divided into C_s and C_c structures, similar to the corresponding A_s and A_c phases. The tilted rods assume an end-to-end spatial arrangement in the C_s phases, whereas the rods form an almost completely interdigitated spatial arrangement in the C_c phase. Similar to the case of the A-phases, it is expected that the parameter β controls the formation of the different C-phases as well. The influence of β

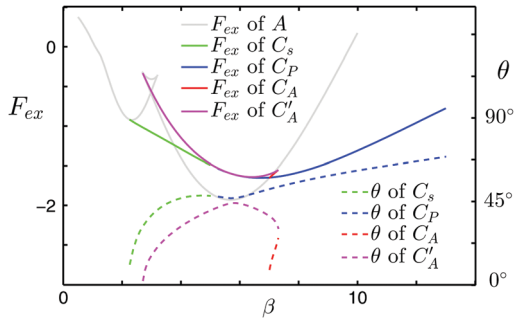

Fig. 4 Plots of the free energy density F_{ex} and the average tilt angle θ of C-phases as a function of β with fixed $\chi N = 15$, $\eta N = 30$, $z_c = 10$.

on the C-phases is revealed in Fig. 4, in which the excess free energy density (F_{ex}) and the average tilt angle (θ) of various C-phases are given as a function of β. The first thing to notice in Fig. 4 is that, as a result of the coupling between the spatial arrangement and orientation of the rods, the free energy curves are more complex than the case of the A-phases. There exist more free energy loops and the average tilt angle θ could be multi-valued. In what follows, for the C_c phase, the case of $\theta > 45^\circ$ is termed the C_P phase (near perpendicular) and the case of $\theta < 45^\circ$ is termed the C_A phase (near the A-phase). It is interesting to note that the example shown in Fig. 4 exhibits three possible values of the tilt angle, labeled by C_P, C_A' and C_A, when β is near 7.2. The C_A' phase is always metastable or unstable, the C_A phase is stable within a very narrow window while the C_P phase is stable within a larger window.

The equilibrium phase of the bilayer is again determined by the minimum of the free energy. For the case shown in Fig. 4, the predicted phase transition sequence is from A_n to A_s to C_s to A_c and to C_c as β is increased. The corresponding tilt angle θ changes from zero for the A-phases to non-zero values for the C-phases.

3.2 Phase diagrams

The phase behaviour of the self-assembled liquid crystalline bilayers is summarized in a set of phase diagrams. The phase diagrams are constructed by a comparison of the excess free energy density of the different candidate phases described above. A typical set of the phase diagrams, plotted in the χN–z_c or ηN–z_c plane, is shown in Fig. 5. The parameter β is chosen to be $\beta = 9.8$ and $\beta = 4$ in accordance with previous studies of the bulk phase behaviour of rod–coil diblock copolymer systems.[22,55]

3.2.1 The case of $\beta = 9.8$. The phase diagrams for the case of a relatively large value of $\beta = 9.8$ are given in Fig. 5(a)–(c). In this case $\beta = 9.8$ is large enough such that the interdigitated arrangement of the rods is the preferred structure. At small values of the activity, z_c, corresponding to low concentration of diblock copolymers, the system is in a disordered or isotropic state in which the rod blocks do not possess liquid crystalline order. Ordered bilayers emerge when z_c is increased beyond a η, χ-dependent critical value. For large values of the ratio η/χ, *e.g.* $\eta N > 22$ with fixed $\chi N = 15$ as shown in Fig. 5(a), the first ordered bilayer is the C_P-phase when z_c is increased. The critical value of z_c exponentially decreases as ηN is increased.

Fig. 5(b) gives the phase diagram with a large ratio $\eta/\chi = 4$. In this case the bilayer structure has an almost horizontal phase transition boundary, $\chi N \approx 6.5$, for $z_c > 4$. That is, the system would change from a disordered state at $\chi N < 6.5$ to a liquid crystalline bilayer at $\chi N > 6.5$. It is interesting to note that this

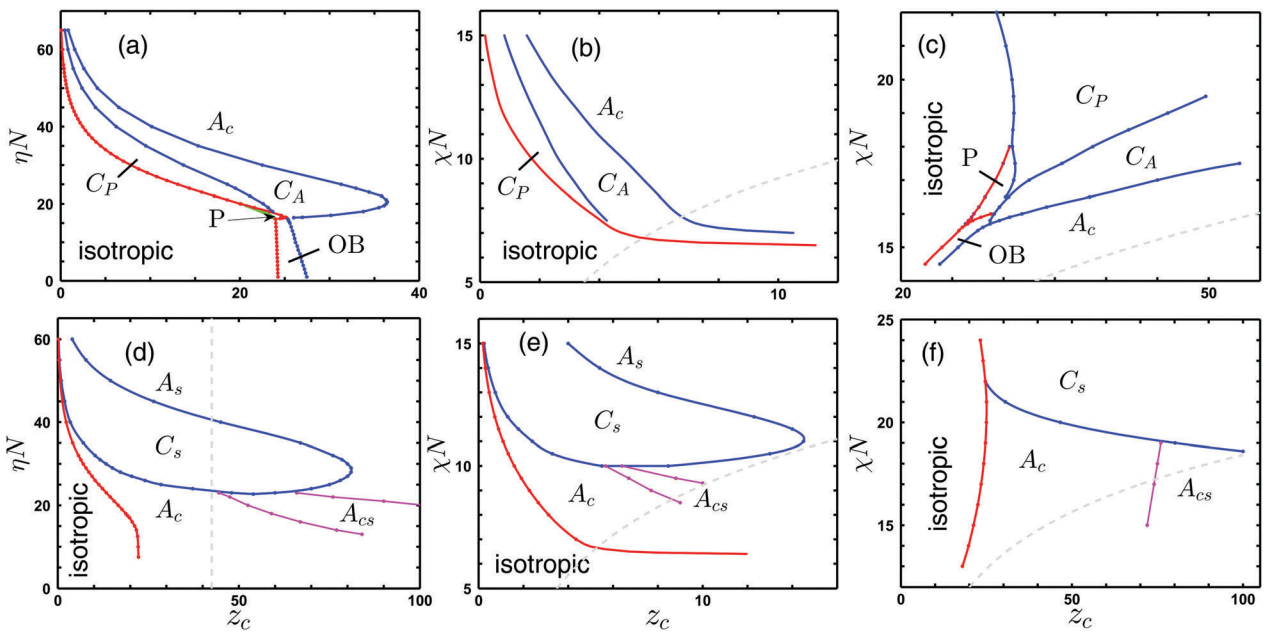

Fig. 5 Phase diagrams of liquid crystalline bilayers. $\beta = 9.8$ for (a–c), (a) $\chi N = 15$, (b) $\eta/\chi = 4$, (c) $\eta/\chi = 1$. $\beta = 4$ for (d–f), (d) $\chi N = 15$, (e) $\eta/\chi = 4$, (f) $\eta/\chi = 1$. To make the region of A-phases more precise, we regard the A_c-phase as the thickness $\Omega/R_g < 1.25\beta$, A_s-phase as $1.5\beta < \Omega/R_g < 2.1\beta$, and the A_{cs}-phase as $1.25\beta < \Omega/R_g < 1.5\beta$. The dashed lines are $\chi N = 4 \ln z_c$ which is the critical condition of the hA-rich bulk phase having lower free energy than the AB-rich bulk phase.

critical value of χN agrees with the value of the order–disorder transition (ODT) point, χN_{ODT}, of the rod–coil diblock melts.[22,33]

For small values of the ratio η/χ and as z_c is increased, the first ordered bilayer could be the P-phase or the OB-phase. The stability region of these two phases is relatively narrow even at a very small ratio of η/χ = 1, as shown in Fig. 5(c). It is worth mentioning that these two structures are analogous to the smectic-OB and smectic-P phases in rod–coil diblock copolymer melts, where they become metastable or unstable when two-dimensional structures are considered and a large value of η/χ = 4 is used.[55]

The C–A and C–P transitions. When the activity z_c or the diblock copolymer concentration is increased, the tilt angle of the rods in the C_c phase decreases, reaching zero at which the bilayer undergoes a C–A transition from the C_c phase to the A_c phase. When $\eta N < 30$, the tilt angle θ is single-valued and it decreases rapidly when z_c is increased for values of ηN close to 30. A similar rapid decrease had been observed for the rod–coil melt system by Reenders and Brinke using Landau theory.[27] The C–A transition could also be induced by increasing the value of ηN, similar to the case of rod–coil melts.[22]

When multiple metastable C-phases are present, the average tilt angle θ could be multi-valued in certain regions of the phase diagram, *e.g.* $\eta N > 30$ at χN = 15, resulting in a first-order transition from the C_P phase to the C_A phase. Details of this phase transition are revealed for the case of χN = 15 and ηN = 40 in Fig. 6(a), where the excess free energy density F_{ex} and the average tilt angle θ are plotted as a function of z_c. The region with multi-valued θ occurs when z_c is between 5.5 and 7.5, and the stable θ jumps from 59° to 31° at the transition point given by z_c = 6.2.

The tilt angle of the bilayer P-phase is 90°. It is tempting to argue that this phase represents a limiting case of the C_P phase with the largest tilt angle. However, it is observed that the maximal tilt angle of the C_P phase does not reach to 90°. Therefore, the C and P phases are two different liquid crystalline phases which are connected *via* a first-order phase transition. In addition, the symmetry of these two phases is different. The C-phases are uniaxial but the P-phase is biaxial.

The OB–A phase transition. For the OB-phase, the eigenvalue with the maximal amplitude, λ_1, of the orientational order parameter **S** is negative ($\lambda_1(\mathbf{S}) < 0$). The average value of $\lambda_1(\mathbf{S})$ increases when the activity z_c is increased, and it becomes positive at the point when the OB-phase undergoes an OB–A transition to the A-phase. The OB–A transition is a first-order transition as shown in Fig. 6(b) for the case of $\eta N > 16$ and χN = 15. The triangle loop in the free energy curve and the multi-valued feature of the eigenvalue $\lambda_1(\mathbf{S})$ demonstrate clearly the first-order nature of the OB–A transition. The transition point in this case is identified at z_c = 24.5, at which the value of $\lambda_1(\mathbf{S})$ jumps from −0.05 in the OB-phase to 0.22 in the A-phase.

3.2.2 The case of β = 4. The phase diagrams for the case with a smaller β = 4 are shown in Fig. 5(d)–(f). In this case the end-to-end arrangement of the rods is the preferred structure.

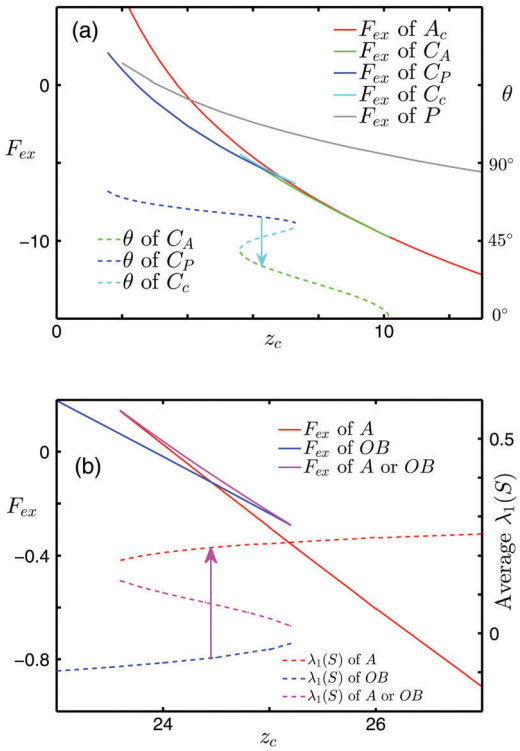

Fig. 6 Free energy and transition of phases. (a) C–A transition and multi-value of the average tilt angle θ (β = 9.8, χN = 15, ηN = 40). (b) OB–A transition with a jump of the average maximal absolute eigenvalue $\lambda_1(\mathbf{S})$ (β = 9.8, χN = 15, ηN = 17).

The first ordered bilayer phase as z_c is increased could be the A_c or C_s phase. Although the phase diagrams for the small β = 4 are quite different from that for the larger β = 9.8, the disorder-to-order transition point is almost the same. In addition, the OB-phase and P-phase are found to be metastable or unstable for this small value of β.

One interesting feature of the phase diagrams shown in Fig. 5(d)–(f) is that the C_s phase is surrounded by the A-phases, resulting in re-entrance A–C–A transitions. It is interesting to note that, for the rod–coil diblock copolymer melts with similar values of β, this type of re-entrance transition has been considered by Halperin.[26] Further theoretical studies by Matsen and Barrett[33] and by Song *et al.*[39] have also confirmed the re-entrance phase transition behaviour in the bulk systems. Qualitative analysis based on the thickness of the bilayer indicates that the A_c phase is preferred at relatively low values of z_c, whereas at large z_c the A_s phase is favoured. However, there is no phase transition between these two structures at small values of ηN because the free energy and bilayer thickness of the A-phases are continuous functions in this case. In the phase diagrams the regions designated as the A_{cs} phase Fig. 5(d–f) are determined by the condition $1.25\beta < \Omega/R_g < 1.5\beta$. It should be noted that these two boundaries are guide to the eyes and they are not phase transition boundaries.

The A–C–A phase transition. As an example of the A_c–C_s–A_s transition when the activity z_c is increased, the excess free

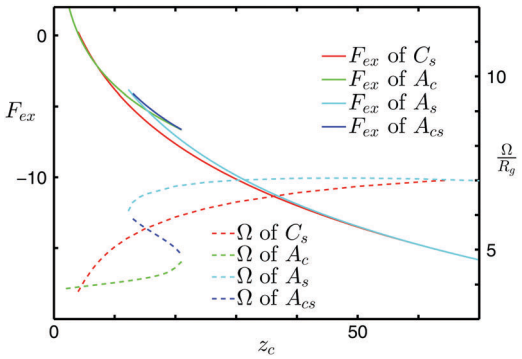

Fig. 7 Plots of the free energy curve and the bilayer thickness curve with $\beta = 4$, $\chi N = 15$, $\eta N = 35$.

energy and the thickness of the bilayer are shown in Fig. 7 for the case of $\chi N = 15$ and $\eta N = 35$. The free energy curve of the A_s and C_s phases is tangent near $z_c = 67$, at which the thickness curves of these two phases merge into one curve, indicating a second-order C_s–A_s transition. On the other hand, it is obvious that the A_c–C_s transition is a first-order transition because their free energy curves crossover with a discontinuity in their slopes.

4 Conclusions and discussion

In summary, the phase behaviour of bilayers self-assembled from rod–coil diblock copolymers is studied using the self-consistent field theory (SCFT) formulated in the grand canonical ensemble. The occurrence and relative stability of various liquid crystalline phases of the bilayers are examined. The theoretical results predict that a variety of ordered structures could become equilibrium phases in the self-assembled bilayers of rod–coil diblock copolymers. The orientational order of rod-blocks within the bilayer could be perpendicular, inclined or parallel to the bilayer, forming ordered membranes of A-phase, C-phase, P-phase and OB-phase. Furthermore, the spatial arrangement of rod blocks could be interdigitated, end-to-end or randomly distributed. A combination of the orientational and spatial arrangements of rod blocks leads to three types of A-phases (A_c, A_s and A_n) and two types of C-phases (C_c and C_s). The transitions between the various A-phases and C-phases could be regulated by increasing the geometrical asymmetry parameter β between the rod blocks and coil blocks, and a phase transition sequence of A_n–A_s–C_s–A_c–C_c is predicted. When β is large enough, the tilt angle of rod-blocks in the C_c-phase could be multi-valued (denoted as C_P and C_A phases). Equilibrium phase diagrams are constructed from the SCFT results by comparing the free energies of various ordered structures. The C_P–C_A–A and A–C–A phase transition paths are predicted by changing the chemical potential or concentration of the copolymers. The results from the theoretical study indicate that the self-assembly of rod–coil diblock copolymer solutions provides a route to obtain nanoscopic bilayers with liquid crystalline order. The ability to control the spatial and orientational arrangements of the rod blocks within a bilayer provides a platform to engineer nano-structured membranes, which could have potential applications in advanced technologies such as photovoltaics.

In this paper we have carried out a detailed theoretical study of the phase behaviour of bilayers self-assembled from rod–coil diblock copolymers. Previous studies of self-assembled bilayers were mostly on the model system composed of coil–coil diblock copolymers and homopolymers, focusing on the elastic properties of the self-assembled bilayers.[24,25,44] Because of the nature of the flexible polymers, the bilayers self-assembled from coil–coil diblock copolymers do not possess internal structures, resulting in fluid or disordered bilayers. In the current study, we focus on the liquid crystalline behaviour of the bilayers self-assembled from rod–coil diblock copolymers. For simplicity, the current study is restricted to the case of $f_A = f_B = 0.5$. Furthermore, we assumed that the bulk phase of the block copolymer/homopolymer mixture is the hA-rich phase, with the bilayers of diblock copolymers self-assembled within the hA-rich homogeneous phase. It is noted that the binary mixture of rod–coil diblock copolymers and homopolymers could have a number of homogeneous phases. In particular, a bulk phase with block copolymers as the majority component becomes the phase with lower free energy when $\chi N > 4 \ln z_c$. This critical line is plotted in the phase diagrams (Fig. 5) for reference. Furthermore, the bulk phase could also possess liquid crystalline order. For example, a bulk nematic phase exists for $\eta N f_B^2 > 6.72$. Previous phase diagrams of the rod–coil systems reveal the narrow window of the stable nematic phase.[22,39] For the cases examined in the current study, the nematic phase is not an equilibrium bulk phase because the homogeneous phases have lower free energy.

One interesting point worth discussing is that a significant number of experiments and theoretical studies have demonstrated that, at low block-copolymer concentrations, the diblock copolymers could self-assemble to form cylindrical and spherical micelles, besides the bilayer structure. For example, Zhou and Shi[42] studied the critical micelle concentration (CMC) of coil–coil diblock copolymers using the SCFT framework in which the cylindrical or spherical micelles have lower CMC than the planar micelles or bilayers when f_A is larger than 0.54. Furthermore, the self-assembly of diblock copolymers within the bilayer could lead to the formation of complex morphologies such as perforated bilayers. It is natural to expect that the rod–coil diblock copolymers could self-assemble to form non-planar micellar structures and compartmentalized layers. Exploring the liquid crystalline order of these complex morphologies and non-planar micelles is a very interesting topic. Another interesting extension of the current study is to go beyond one-dimensional calculations. The coupling between the liquid crystalline order and the bilayer conformation could lead to interesting deformations of the planar bilayers. However, a detailed study of these topics is beyond the scope of the current paper and we will leave this topic to future studies.

Acknowledgements

The authors thank the National Natural Science Foundation of China (Grant No. 11421101 and 11421110001) for financial support. ACS's research is supported by the Natural Sciences and Engineering Research Council (NSERC) of Canada. The computation

was made possible by the facilities of the Shared Hierarchical Academic Research Computing Network (SHARCNET).

References

1 I. W. Hamley, *Developments in Block Copolymer Science and Technology*, Wiley Online Library, 2004.
2 F. S. Bates, M. A. Hillmyer, T. P. Lodge, C. M. Bates, K. T. Delaney and G. H. Fredrickson, *Science*, 2012, **336**, 434–440.
3 C. M. Bates and F. S. Bates, *Macromolecules*, 2017, **50**, 3–22.
4 A.-C. Shi and B. Li, *Soft Matter*, 2013, **9**, 1398–1413.
5 C. Wang, Y. Xu, W. Li and Z. Lin, *Langmuir*, 2016, **32**, 7908–7916.
6 M. Byun, W. Han, B. Li, X. Xin and Z. Lin, *Angew. Chem.*, 2013, **52**, 1122–1127.
7 B. D. Olsen and R. A. Segalman, *Mater. Sci. Eng., R*, 2008, **62**, 37–66.
8 G. Yang, P. Tang, Y. Yang and Q. Wang, *J. Phys. Chem. B*, 2010, **114**, 14897–14906.
9 Y.-B. Lim, K.-S. Moon and M. Lee, *J. Mater. Chem.*, 2008, **18**, 2909–2918.
10 J. Zhang, X.-F. Chen, H.-B. Wei and X.-H. Wan, *Chem. Soc. Rev.*, 2013, **42**, 9127–9154.
11 L.-Y. Shi, Y. Zhou, X.-H. Fan and Z. Shen, *Macromolecules*, 2013, **46**, 5308–5316.
12 M. Lee, B.-K. Cho and W.-C. Zin, *Chem. Rev.*, 2001, **101**, 3869–3892.
13 J. Chen, E. Thomas, C. Ober and G.-P. Mao, *Science*, 1996, **273**, 343–346.
14 M. He, F. Qiu and Z. Lin, *J. Mater. Chem.*, 2011, **21**, 17039–17048.
15 Y. Lee and E. Gomez, *Macromolecules*, 2015, **48**, 7385–7395.
16 S. A. Safran, *Statistical Thermodynamics of Surfaces, Interfaces, and Membranes*, Addison-Wesley, New York, 1994.
17 A. Taubert, A. Napoli and W. Meier, *Curr. Opin. Chem. Biol.*, 2004, **8**, 598–603.
18 A. Mecke, C. Dittrich and W. Meier, *Soft Matter*, 2006, **2**, 751–759.
19 A. Tardieu, V. Luzzati and F. C. Reman, *J. Mol. Biol.*, 1973, **75**, 711–733.
20 A. N. Semenov, *Mol. Cryst. Liq. Cryst.*, 1991, **209**, 191–199.
21 B. D. Olsen and R. A. Segalman, *Macromolecules*, 2005, **38**, 10127–10137.
22 W. Song, P. Tang, F. Qiu, Y. Yang and A.-C. Shi, *Soft Matter*, 2011, **7**, 929–938.
23 M. Müller, K. Katsov and M. Schick, *Phys. Rep.*, 2006, **434**, 113–176.
24 J. Li, K. Pastor, A.-C. Shi, F. Schmid and J. Zhou, *Phys. Rev. E: Stat., Nonlinear, Soft Matter Phys.*, 2013, **88**, 012718.
25 P.-W. Zhang and A.-C. Shi, *Chin. Phys. B*, 2015, **24**, 45–52.
26 A. Halperin, *Europhys. Lett.*, 1989, **10**, 549–553.
27 M. Reenders and G. Brinke, *Macromolecules*, 2002, **35**, 3266–3280.
28 M. A. Horsch, Z. Zhang and S. C. Glotzer, *Phys. Rev. Lett.*, 2005, **95**, 056105.
29 S. Dolezel, H. Behringer and F. Schmid, *Polym. Sci., Ser. C*, 2013, **55**, 70–73.
30 W. Li and D. Gersappe, *Macromolecules*, 2001, **34**, 6783–6789.
31 J. Chen, C. Zhang, Z. Sun, Y. Zheng and L. An, *J. Chem. Phys.*, 2006, **124**, 104907.
32 M. Müller and M. Schick, *Macromolecules*, 1996, **29**, 8900–8903.
33 M. W. Matsen and C. Barrett, *J. Chem. Phys.*, 1998, **109**, 4108–4118.
34 V. Pryamitsyn and V. Ganesan, *J. Chem. Phys.*, 2004, **120**, 5824–5838.
35 B. D. Olsen, M. Shah, V. Ganesan and R. A. Segalman, *Macromolecules*, 2008, **41**, 6809–6817.
36 J. Gao, W. Song, P. Tang and Y. Yang, *Soft Matter*, 2011, **7**, 5208–5216.
37 J. Tang, Y. Jiang, X. Zhang, D. Yan and J. Z. Y. Chen, *Macromolecules*, 2015, **48**, 9060–9070.
38 H. Wu, L. He, X. Wang, Y. Wang and Z. Jiang, *Soft Matter*, 2014, **10**, 6278–6285.
39 W. Song, P. Tang, F. Qiu, Y. Yang and A.-C. Shi, *J. Phys. Chem. B*, 2011, **115**, 8390–8400.
40 Y. Tao, B. D. Olsen, V. Ganesan and R. A. Segalman, *Macromolecules*, 2007, **40**, 3320–3327.
41 G. H. Fredrickson, *The Equilibrium Theory of Inhomogeneous Polymers*, Oxford University Press, Oxford, 2006.
42 J. Zhou and A.-C. Shi, *Macromol. Theory Simul.*, 2011, **20**, 690–699.
43 M. W. Matsen, *Macromolecules*, 1995, **28**, 5765–5773.
44 M. Laradji and R. C. Desai, *J. Chem. Phys.*, 1998, **108**, 4662–4674.
45 P. Flory, *Principles of Polymer Chemistry*, Cornell University Press, Ithaca, New York, 1953.
46 W. Maier and A. Saupe, *Z. Naturforsch.*, 1958, **13A**, 564–566.
47 J. Yu, F. Liu, P. Tang, F. Qiu, H. Zhang and Y. Yang, *Polymers*, 2016, **8**, 184.
48 R. B. Thompson, K. O. Rasmussen and T. Lookman, *J. Chem. Phys.*, 2004, **120**, 31–34.
49 D. Düchs and D. E. Sullivan, *J. Phys.: Condens. Matter*, 2002, **14**, 12189–12202.
50 W. Song, P. Tang, H. Zhang, Y. Yang and A.-C. Shi, *Macromolecules*, 2009, **42**, 6300–6309.
51 S. K. Lele, *J. Comput. Phys.*, 1992, **103**, 16–42.
52 J. C. Butcher, *Numerical Methods for Ordinary Differential Equations*, Springer-Verlag, 2nd edn, 2008.
53 W. Xu, K. Jiang, P. Zhang and A.-C. Shi, *J. Phys. Chem. B*, 2013, **117**, 130417155037004.
54 A. Arora, J. Qin, D. C. Morse, K. T. Delaney, G. H. Fredrickson, F. S. Bates and K. D. Dorfman, *Macromolecules*, 2016, **49**, 4675–4690.
55 Q. Liang, PhD thesis, Peking University, 2012.